

**Climatology, seasonality and trends of oceanic coherent
eddies**

Josué Martínez-Moreno¹, Andrew McC. Hogg¹, and Matthew England²

⁴ Research School of Earth Science and ARC Center of Excellence for Climate Extremes, Australian
⁵ National University, Canberra, Australia

⁶ Climate Change Research Centre (CCRC), UNSW Australia, Sydney NSW, Australia

Key Points:

- ⁸ Kinetic energy of coherent eddies contain around 30% of the surface ocean kinetic
⁹ energy budget.
- ¹⁰ Seasonal cycle of the number of coherent eddies and coherent eddy amplitude re-
¹¹ veal a 3-6 month lag to wind forcing
- ¹² The coherent eddy amplitude has increase at a rate of 3 cm per decade since 1993.

13 **Abstract**

14 Ocean eddies influence regional and global climate through mixing and transport
 15 of heat and properties. One of the most recognizable and ubiquitous feature of oceanic
 16 eddies are vortices with spatial scales of tens to hundreds of kilometers, frequently re-
 17 ferred as “mesoscale eddies” or “coherent eddies”. Coherent eddies are known to trans-
 18 port properties across the ocean and to locally affect near-surface wind, cloud proper-
 19 ties and rainfall patterns. Although coherent eddies are ubiquitous, yet their climatol-
 20 ogy, seasonality and long-term temporal evolution remains poorly understood.

21 Thus, we examine the kinetic energy contained by coherent eddies and we present
 22 the annual, interannual, and long-term changes of automatically identified coherent ed-
 23 dies from satellite observations and a state of the art numerical simulation from 1993 to
 24 2018. Satellite observations show that around 40% of the kinetic energy contained by
 25 ocean eddies corresponds to coherent eddies. Additionally, a strong hemispherical sea-
 26 sonal cycle is observed, on top of a 3–6 months lag between the wind forcing and the re-
 27 sponse of the coherent eddy field. Furthermore, the seasonality of the number of coher-
 28 ent eddies and their amplitude reveals that the number of coherent eddies responds faster
 29 to the forcing (~ 3 months), while the coherent eddy amplitude is lagged by ~ 6 months.
 30 There are regions that show a pronounced influence of coherent eddies, notably, the East
 31 Indian Ocean, the East Tropical Pacific Ocean, and the South Atlantic Ocean. In these
 32 locations, a strong seasonal cycle and interannual variability can be observed in both satel-
 33 lite and numerical models. Although, there is agreement between these products on the
 34 seasonality of the number of eddies, the seasonality of the coherent eddy amplitude be-
 35 tween these products show some inconsistencies. Long-term trends of the coherent eddy
 36 amplitude from satellite observations and the state of the art model show significant in-
 37 creases in the eddy amplitude of $\sim 3\text{cm}$ per decade in large portions of the ocean, while
 38 the number of coherent eddies remains constant. Our analysis highlight the relative im-
 39 portance of the coherent eddy field in the ocean kinetic energy budget, imply a strong
 40 response of the eddy number and eddy amplitude to the surface wind at different time-
 41 scales, and showcases for the first time seasonality, and multidecadal trends of the co-
 42 herent eddy properties.

43 **Plain language summary**

44 1 Introduction

45 Mesoscale ocean variability with spatial scales of tens to hundreds of kilometers is
 46 comprised of processes such as vortices, waves, and jets (Ferrari & Wunsch, 2009; Fu et
 47 al., 2010). These mesoscale processes are highly energetic, and they play a crucial role
 48 in the transport of heat, salt, momentum, and other tracers through the ocean (Wun-
 49 sch & Ferrari, 2004; Wyrtki et al., 1976; Gill et al., 1974). Possibly, the most recogniz-
 50 able and abundant process observed from satellites is mesoscale vortices. Although mesoscale
 51 vortices are commonly referred to in literature as “mesoscale eddies”, this term is also
 52 often used to describe mesoscale ocean variability (time-varying component of flow), thus,
 53 here we will refer to mesoscale vortices as coherent eddies.

54 Coherent eddies are circular currents and according to their rotational direction,
 55 the sea surface height anomaly within a coherent eddy can have a negative or positive
 56 sea surface height anomaly (cold-core and warm-core coherent eddies, respectively). This
 57 characteristic sea surface height signature of coherent eddies has been utilized to auto-
 58 matically identified and tracked coherent eddies from satellite altimetry (Cui et al., 2020;
 59 Martínez-Moreno et al., 2019; Ashkezari et al., 2016; Faghmous et al., 2015; Chelton et
 60 al., 2007). Automated identification algorithms of coherent eddies have shown their ubiq-
 61 uity in the oceans, with a predominant influence at hotspots of eddy activity such as bound-
 62 ary currents and the Antarctic Circumpolar Current. In these regions, Chelton et al. (2011)
 63 estimated that coherent eddies contribute around 40–50% of the mesoscale kinetic en-
 64 ergy (Chelton et al., 2011) and thus a significant fraction of the total kinetic energy (Fer-
 65 rari & Wunsch, 2009). Although this unique estimate showcases the importance of the
 66 mesoscale coherent eddy field, the energy contained by coherent eddies was estimated
 67 by extracting the geostrophic velocities within the detected coherent eddies, thus it is
 68 possible it may contain energy from other processes. Coherent eddies are not only abun-
 69 dant and may have a large proportion of the surface kinetic energy budget, but they also
 70 are essential in the ocean dynamics as concluded by many previous studies (Patel et al.,
 71 2020; Schubert et al., 2019; Pilo et al., 2015; Frenger et al., 2015, 2013; Beron-Vera et
 72 al., 2013; Siegel et al., 2011; Hogg & Blundell, 2006).

73 There is broad consensus that mesoscale eddy kinetic energy has a pronounced sea-
 74 sonal variability (Uchida et al., 2017; Kang & Curchitser, 2017; Qiu & Chen, 2004; Qiu,
 75 1999), several hypotheses proposed to explain this include: seasonal variations of atmo-

spheric forcing (Sasaki et al., 2014), seasonality of the mixed layer depth (Qiu et al., 2014; Callies et al., 2015), seasonality in the intensity of barotropic instability (Qiu & Chen, 2004), the variability of the baroclinic instability due to the seasonality of the vertical shear (Qiu, 1999), and a seasonal lag of the inverse energy cascade (energy is transported between scales from small to large; Arbic et al., 2013) in combination with the presence of a front in the mixed layer, which can lead to a seasonal cycle of the baroclinic instability (Qiu et al., 2014). All these factors are likely to influence the seasonal cycle of coherent eddies, however, the seasonality of the coherent component of the eddy kinetic energy, as well as the seasonal cycle of the coherent eddy statistics remains unknown.

On one hand, processes such as barotropic and baroclinic instabilities could control the seasonality of coherent eddies in the ocean. On the other hand, recent studies using observations and eddy-permitting climate models suggest several long-term adjustments of the global ocean capable of long-term changes in the coherent eddy field. Such readjustments include a multidecadal increase in the ocean stratification resulted from temperature and salinity changes (Li et al., 2020), a horizontal readjustment of the sea surface temperature gradients (Ruela et al., 2020; Bouali et al., 2017; Cane et al., 1997), and an intensification of the kinetic energy, eddy kinetic energy, and mesoscale eddy kinetic energy over the last 3 decades as a consequence of an increase in wind forcing (Hu et al., 2020; Wunsch, 2020; Martínez-Moreno et al., 2021). These readjustments are directly tight with the generation of coherent eddies, thus they could modify the long-term response of the mesoscale coherent eddy field.

Andy suggested moving the previous paragraph somewhere else, but I don't know where would it fit best, I think it will be confusing to introduce long-term trends before the seasonal cycle. Any suggestion? Perhaps merge both paragraphs? i.e. . . . of the baroclinic instability (Qiu et al., 2014). On one hand, processes such as barotropic and baroclinic instabilities could control the seasonality of coherent eddies in the ocean. On the other hand, recent studies . . . All these seasonal factors and long-term readjustments directly influence the annual and decadal response of the coherent eddy field, however, the seasonality of the coherent component of the eddy kinetic energy, as well as the seasonal cycle and trends of the coherent eddy statistics remain unknown. What do you think?

Here we present a new estimate and climatology of the coherent eddy kinetic energy by reconstructing the coherent eddy signature from satellite observations, the seasonal cycle of the coherent eddy kinetic energy, and seasonal cycle and long-term trends

of the coherent eddy properties over the satellite record. Moreover, we investigate regions where coherent eddies dominate the eddy kinetic energy field. This paper is structured as follows: the data sources and methodology are described in section 2. Then, we present the climatology, energy ratios, and global seasonality of the coherent eddy kinetic energy in subsection 3. Subsection 4 presents the global climatology and seasonality of coherent eddy properties, followed by the seasonal cycle and coherent eddy property time-series in regions dominated by coherent eddies (subsection 6.1). We then focus our attention on the long-term changes of the coherent eddy properties (section 5). Finally, section 7 summarizes the main results and discusses the implications of this study.

2 Methods

2.1 Data

We use daily sea surface height (SSH) data available by the Copernicus Marine Environment Monitoring Service in near real time (CMEMS, 2017). This gridded product contains the sea surface height and geostrophic velocities with daily 0.25° resolution from January 1993 to 2019. The daily geostrophic velocities allowed us to compute the KE and EKE over the satellite records. Mean and anomaly velocities are in reference to the full record mean of SSH (1993–2019), while all presented climatologies correspond to the mean of the full record.

Over the same record, we use a mesoscale coherent eddy trajectory dataset released by Chelton and Schlax (2013) to compare global statistics of coherent eddies in the present study. This dataset was produced via an automated eddy identification developed by Chelton et al. (2011).

The eddy identification procedure defines mesoscale eddies directly using the sea surface height (SSH) field. This method was applied to avoid noise amplification in the SSH field. Compared with the Okubo–Weiss parameter identification procedure, the SSH-based procedure without the differentiation calculation of the SSH field effectively solves the overestimation issue of eddy identification with less computational load. The dataset retains only those eddies with lifetimes of four weeks or longer and provides trajectories with 7-day time steps

Wind stress averaged over oceanic regions between 45S and 65S calculated from the ERA interim reanalysis [Dee et al., 2011] (Figure 1b, black line) correlates well with

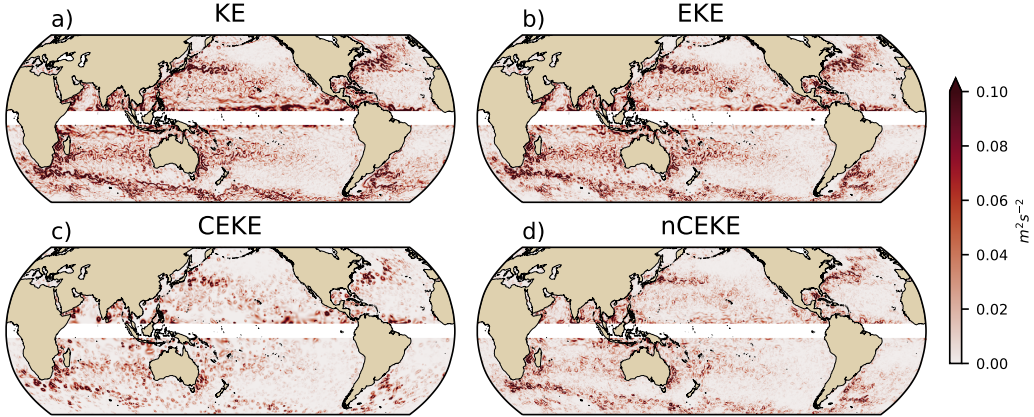
139 the annually averaged SAM (correlation 0.88). Wind stress increases from 1990 onward
 140 at a rate consistent with the long-term trend (not shown) albeit masked by strong lev-
 141 els of interannual variability. We also show how the ERA-interim wind stress has var-
 142 ied within each ocean basin (Figure 1c). For this, we divide the Southern Ocean up into
 143 the three sectors similar to those used by MH06 (Indian Ocean: 40E–150E, 57S–44S; Pa-
 144 cific Ocean: 150E–288E, 62S–48S; and Atlantic Ocean: 325E–10E, 56S–46S). The regional
 145 analysis indicates that the long-term trend in Southern Ocean wind stress is dominated
 146 by changes in the Pacific sector.

147 2.2 Coherent eddy identification algorithm

148 TrackEddy is an autonomous eddy identification, tracking, and reconstruction al-
 149 gorithm, which assumes eddies can be represented as isolated anisotropic Gaussian anom-
 150 lies. The main and unique characteristic of the TrackEddy algorithm, which differs from
 151 previous algorithms (Ashkezari et al., 2016; Chelton et al., 2007; Faghmous et al., 2015),
 152 is its capability to reconstruct an optimal Gaussian anomaly for each identified eddy. This
 153 Gaussian anomaly can be used to reconstruct the eddy velocities to calculate the TKE
 154 associated with the identified coherent eddies. TrackEddy follows a similar work-flow to
 155 previous methods using SSH. It starts with a single snapshot of SSHa, where potential
 156 eddies are isolated using study-specific criteria. Generally, each study describes a strict
 157 definition of what will be considered an eddy by constraining their size and/or shape.
 158 Then, the algorithm iterates at multiple discrete SSHa levels in which the coherent eddy
 159 definition is used to identify eddies. The identification algorithm at each discrete SSHa
 160 level is then applied to all time steps for which data are available. The following sub-
 161 sections present the TrackEddy algorithm structure, criteria, user-specified values, and
 162 energy calculation.

163 2.3 Kinetic Energy decomposition

164 Kinetic energy is commonly divided into the mean and time-varying components
 165 through a Reynolds decomposition. At a given time, the velocity field $\mathbf{u} = (u, v)$ is split
 166 into the time mean ($\bar{\mathbf{u}}$) and time varying components (\mathbf{u}'). Additionally, we further de-
 167 compose the eddy kinetic energy into the eddy kinetic energy contained by coherent fea-
 168 tures (\mathbf{u}_e') and non-coherent (\mathbf{u}_n'). Therefore the KE equation can be written as:



175 **Figure 1.** Snapshot of surface kinetic energy (\overline{KE}), surface eddy kinetic energy (\overline{EKE}),
 176 surface coherent eddy kinetic energy (\overline{CEKE}), and surface non-coherent eddy kinetic energy
 177 (\overline{nCEKE}) for the 1st of January 2017.

$$KE = \underbrace{\bar{u}^2 + \bar{v}^2}_{MKE} + \underbrace{u_e'^2 + v_e'^2}_{CEKE} + \underbrace{u_n'^2 + v_n'^2}_{nCEKE} + \mathcal{O}_c^2 + \mathcal{O}^2 \quad (1)$$

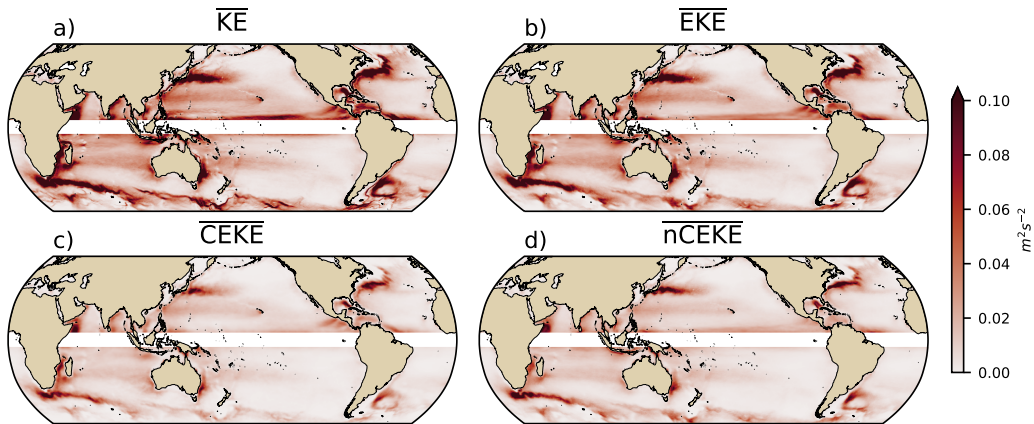
169 Due to the properties of this decomposition, the second order term \mathcal{O}^2 is zero when av-
 170 eraged over the same period as \bar{u} . However, \mathcal{O}_c^2 is only negligible when averaged in time
 171 and space. For more information about the decomposition of the field into coherent fea-
 172 tures and non-coherent features refer to Martínez-Moreno et al. (2019). A global snap-
 173 shot of each component of kinetic energy decomposition is shown in figure 1, where the
 174 imprint of the coherent eddies corresponds to rings of kinetic energy.

178 3 Global Coherent Eddy Energetics

179 **Figure 2**

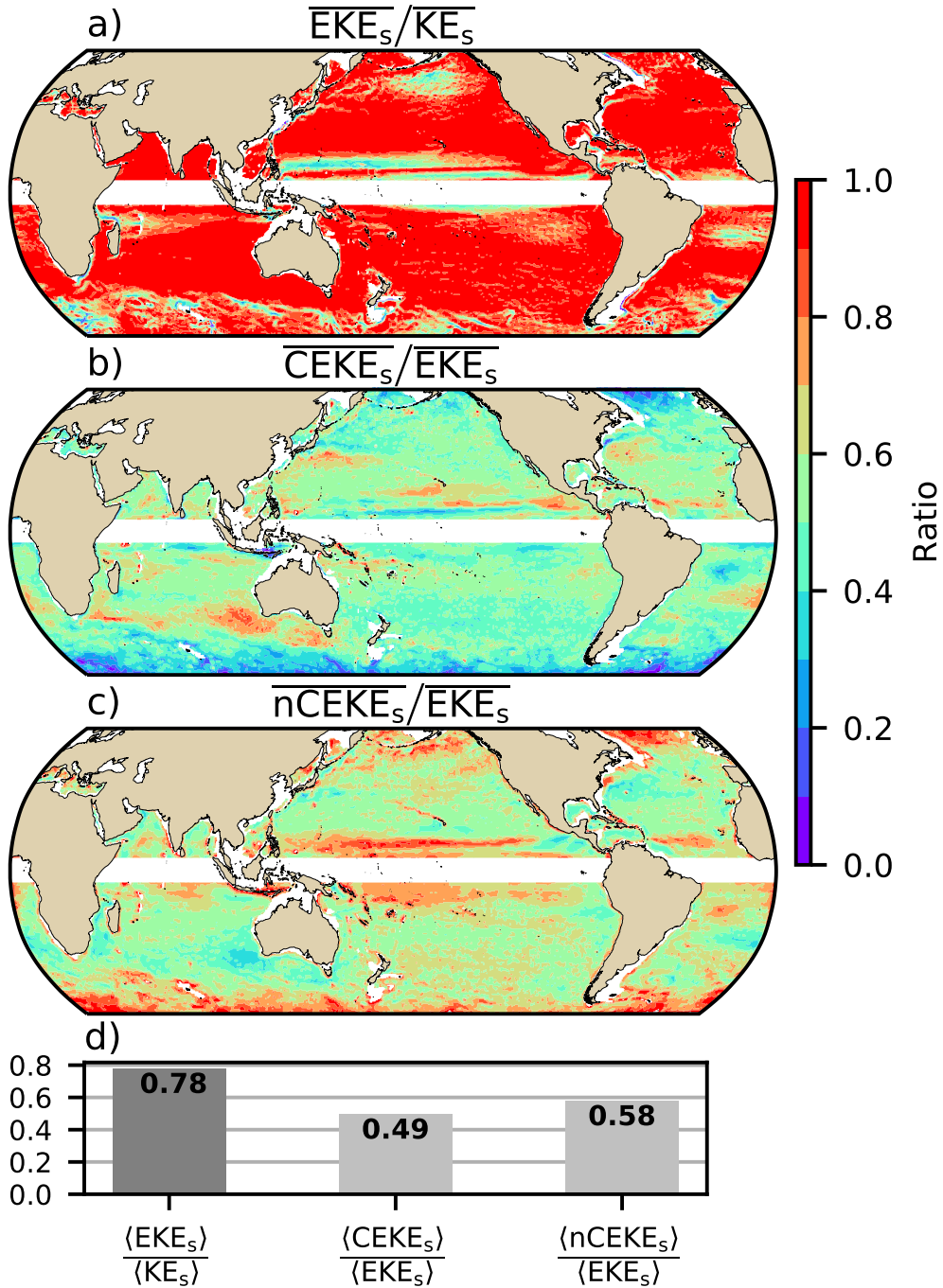
- 180 • All KE components have large energy contents in the boundary currents and antarc-
 181 tic circumpolar current.
- 182 • In many cases is the same, but there actually some differences There are several
 183 regions where the coherent component is larger than the non-coherent, we will in-
 184 vestigate these in more detail in section XX.

188 **Figure 3**



185 **Figure 2.** Climatology of surface kinetic energy (\overline{KE}), surface eddy kinetic energy (\overline{EKE}),
 186 surface coherent eddy kinetic energy (\overline{CEKE}), and surface non-coherent eddy kinetic energy
 187 (\overline{nCEKE}) between 1993-2018.

- 189 • \overline{EKE} is responsible of almost all the \overline{KE} across the ocean, except for regions with
 190 persistent currents over time, such as the mean boundary current locations, equa-
 191 torial pacific currents and regions in the Antarctic Circumpolar current, where the
 192 EKE explains around 40% of the \overline{KE}
- 193 • This estimate is consistent with that of Chelton.
- 194 • \overline{EKE} Explains 80% of \overline{KE} , while \overline{CEKE} is 45% of \overline{EKE} and \overline{nCEKE} is 60% of
 195 \overline{EKE}
- 196 • \overline{CEKE} is large equatorwards from the Kuroshio current and Agulhas current.
- 197 • Areas with the largest coherent contribution are located in the South of Australia
 198 \overline{CEKE} and South Atlantic
- 199 •
- 200 • \overline{nCEKE} has a large amount of energy at high latitudes, this could be a consequence
 201 of the satellites not resolving the mesoscale coherent eddies.
- 202 • Global averages of the ratios show \overline{EKE} explains around 78% of the ocean *MKE*
 203 field, while coherent eddies and non coherent eddy features contain 49% and 59%
 204 per decade. Note this values don't add to 1 as there are cross terms that contain
 205 around XX% of the total energy.



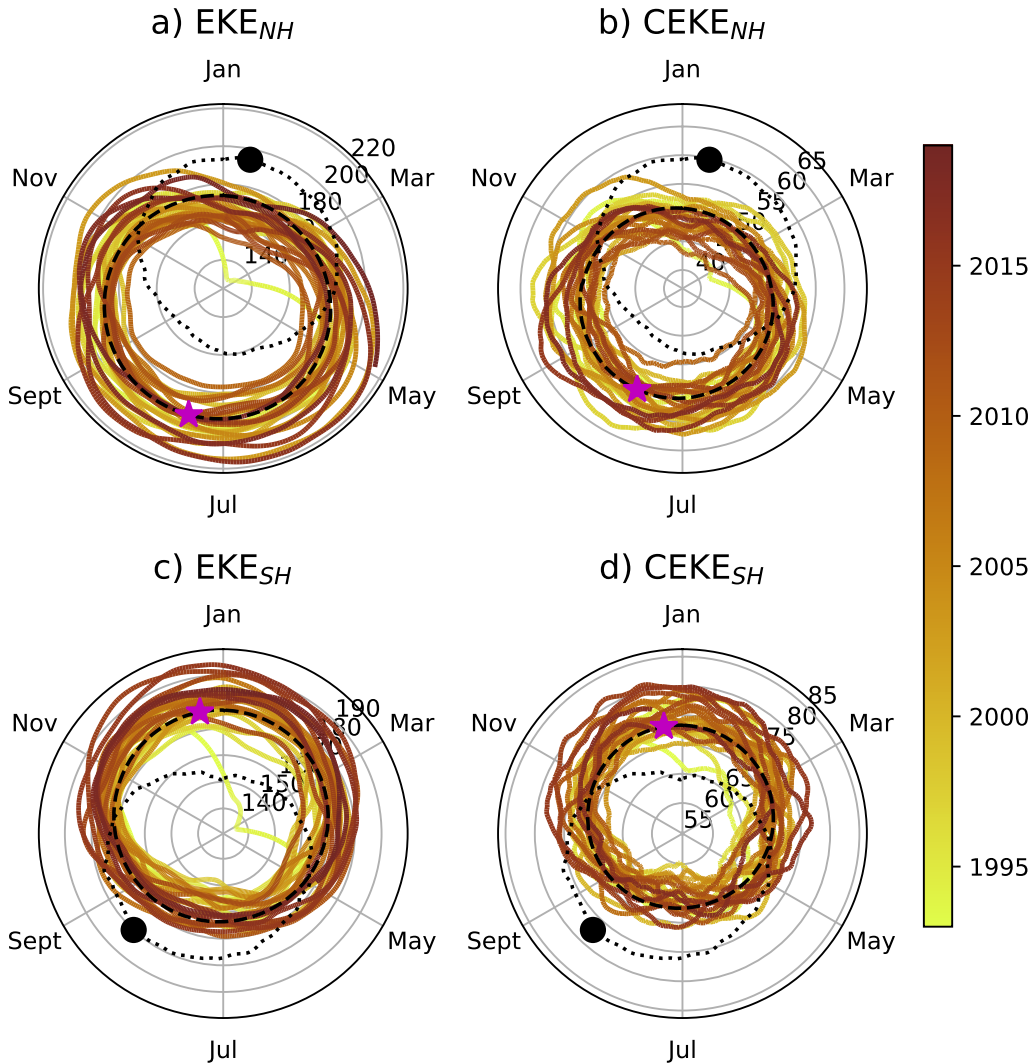
206 **Figure 3.** Ratios of the kinetic energy components. a) Map of the proportion of mean eddy
 207 kinetic energy (EKE_s) versus mean kinetic energy (\overline{KE}); b) Map of the percentage of mean co-
 208 herent eddy kinetic energy (\overline{CEKE}_s) versus mean eddy kinetic energy (\overline{EKE}_s); c) Map of the
 209 percentage of mean non-coherent eddy kinetic energy (\overline{nCEKE}_s) versus mean eddy kinetic energy
 210 (\overline{EKE}_s); d) Global averaged percentage of mean eddy kinetic energy ($\langle \overline{EKE} \rangle$) versus the global
 211 mean kinetic energy ($\langle \overline{KE} \rangle$), and percentage of mean coherent eddy kinetic energy ($\langle \overline{CEKE} \rangle$)
 212 and mean non coherent eddy kinetic energy ($\langle \overline{nCEKE} \rangle$) versus global mean eddy kinetic energy
 213 ($\langle \overline{EKE} \rangle$).

214 **3.0.1 Seasonality**215 **Figure 4**

- 216 • The hemisphere seasonality show the EKE and CEKE peak in summer.
- 217 • Response of the EKE and CEKE show a seasonal lag of ~6 months to the forc-
- 218 ing of the Winds. Make sure to note the maximum over the hemisphere, locally,
- 219 the winds may peak in different months.
- 220 • Methods, explain more about winds or here.
- 221 • The coherent eddy field show a large interannual variability.
- 222 • In the Southern Ocean we observe a concentric growth as time passes, which sup-
- 223 port the increasing trends in the Southern Ocean observed by (Hogg et al., 2015;
- 224 Martínez-Moreno et al., 2019, 2021)
- 225 • Point that in the northern hemisphere in winter the CEKE appears to be decreas-
- 226 ing.

233 **4 Global Coherent Eddy Statistics**234 **Figure 5**

- 235 • A comparison with previous identified numbers show a consistent pattern in the
- 236 eddy count. The difference in the magnitude could be a consequence of Chelton
- 237 et al. (2007) filtering the coherent eddies with lifespans longer than 16 weeks.
- 238 • Both datasets show a large number of eddies in the East North Pacific, East North
- 239 Atlantic, as well as the East South Pacific, East South Atlantic and East Indian
- 240 Ocean.
- 241 • While the number of eddies detected in the tropics is quite small.
- 242 • Furthermore, there are hotspots of numbers of eddies in other regions of the ocean,
- 243 such as boundary currents and the Antarctic Circumpolar Current.
- 244 • An interesting feature shown in both datasets is a predominant patchiness where
- 245 the count of the eddies is much larger. These puzzling pattern remains unknown.
- 246 Although it looks like a propagation pattern, it could be that eddies persist for
- 247 longer in those areas.
- 248 • The eddy amplitude as expected is maximum at the boundary currents and hotspots
- 249 in the southern ocean.



227 **Figure 4.** Hemispherical seasonality of eddy kinetic energy (EKE), coherent eddy kinetic en-
 228 ergy (CEKE). Panels a, and b show the northern hemisphere seasonal cycle, while panels c, and
 229 d correspond to the southern hemisphere. Dashed lines correspond to the seasonal cycle of the
 230 fields and dotted lines show the seasonal cycle of the wind magnitude smoothed over 120 days
 231 (moving average). The green and magenta stars show the maximum of the seasonal cycle for the
 232 kinetic energy components and the wind magnitude, respectively. The line colors show the year.

- 250 • Interior of the gyres we can observe that there is an important amplitude of the
251 coherent eddy field.
- 252 • Preferred eddy amplitude sign in boundary currents; positive amplitude polewards
253 to the boundary current mean location, and negative amplitude equatorwards. This
254 is consistent with the shed of coherent eddies from the boundary currents.
- 255 • There regions with large CEKE ratio show also a large coherent eddy amplitude.
- 256 • Absolute eddy amplitude has the similar signature as CEKE.

262 *4.0.1 Seasonality*

263 **Figure 6**

- 264 • Seasonality of the number of eddies in the Northern Hemisphere peaks on May,
265 while the Southern Hemisphere peaks on October.
- 266 • The seasonality of the amplitude of the eddies is consistent with those of the Co-
267 herent eddy kinetic energy.
- 268 • Interestingly, there is a 3 month lag between the winds and the seasonality of
269 the number of eddies, while the eddy amplitude responds approximately 6 months
270 after the maximum winds.
- 271 • Note that both coherent eddy amplitudes seem to peak around the same time.
- 272 • If we look closely, the growing-shrinking concentric circles correspond to an increasing-
273 decreasing trend. These are particularly obvious as a decrease in the eddy num-
274 ber in the Southern Hemisphere, and an increase in the eddy amplitude.

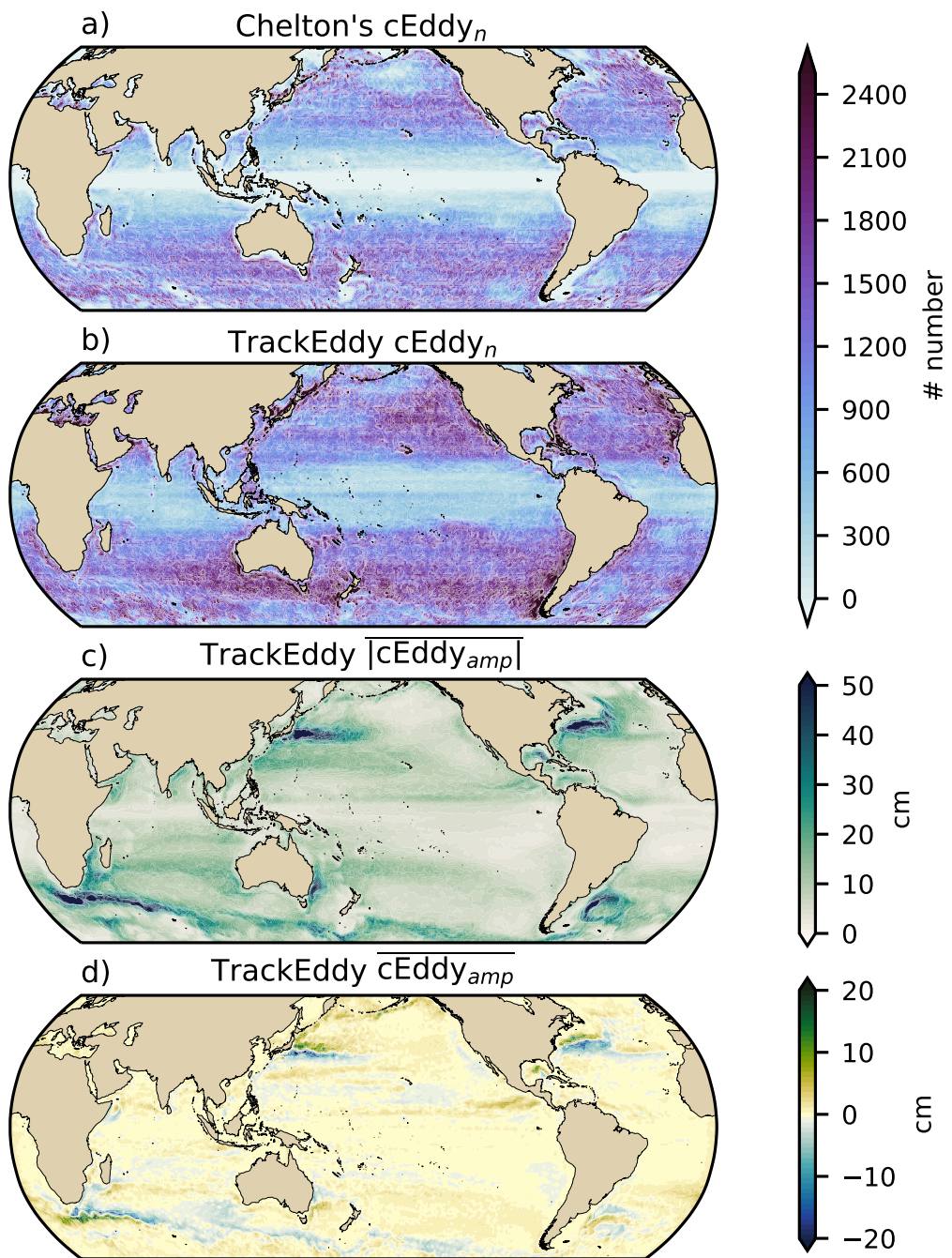
284 **Figure 6**

- 285 • a

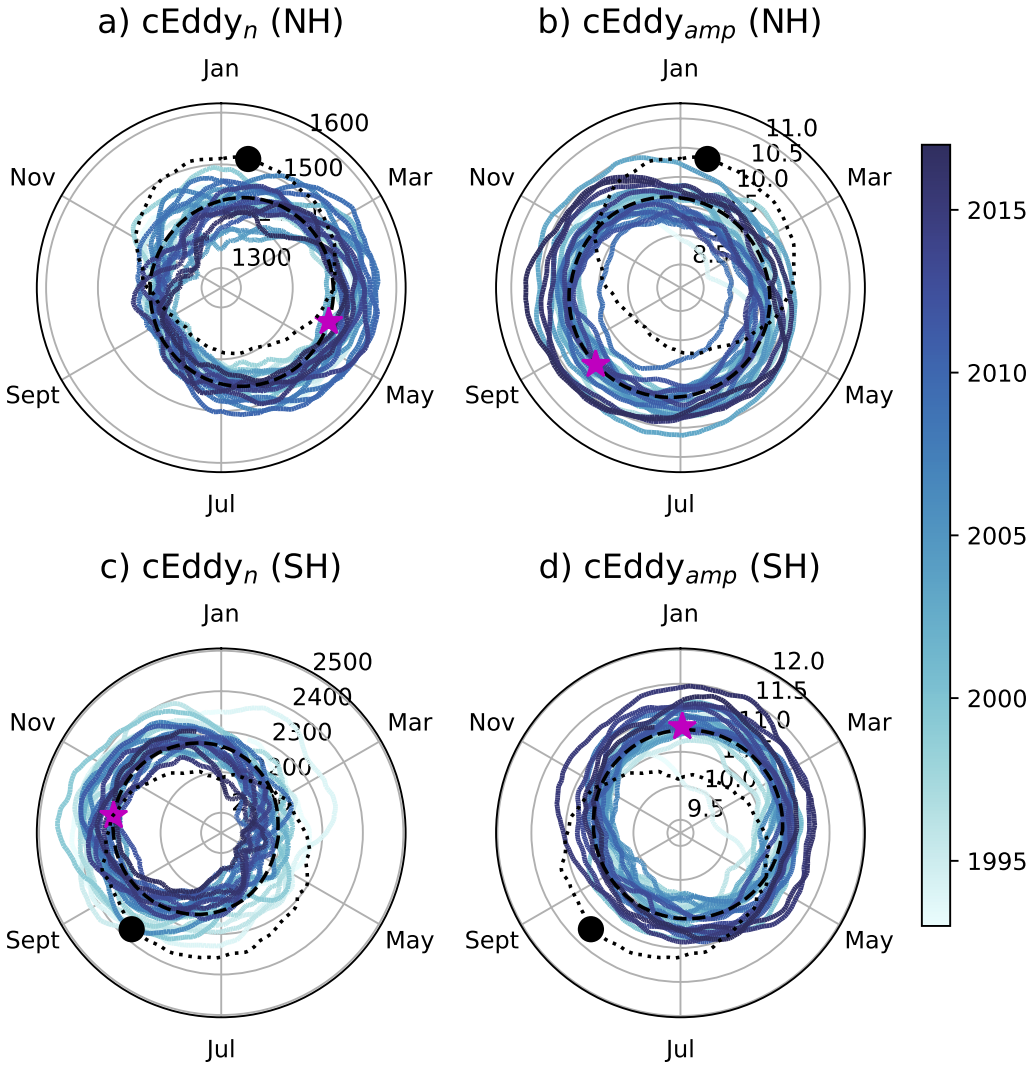
295 **5 Trends**

296 **Figure 13**

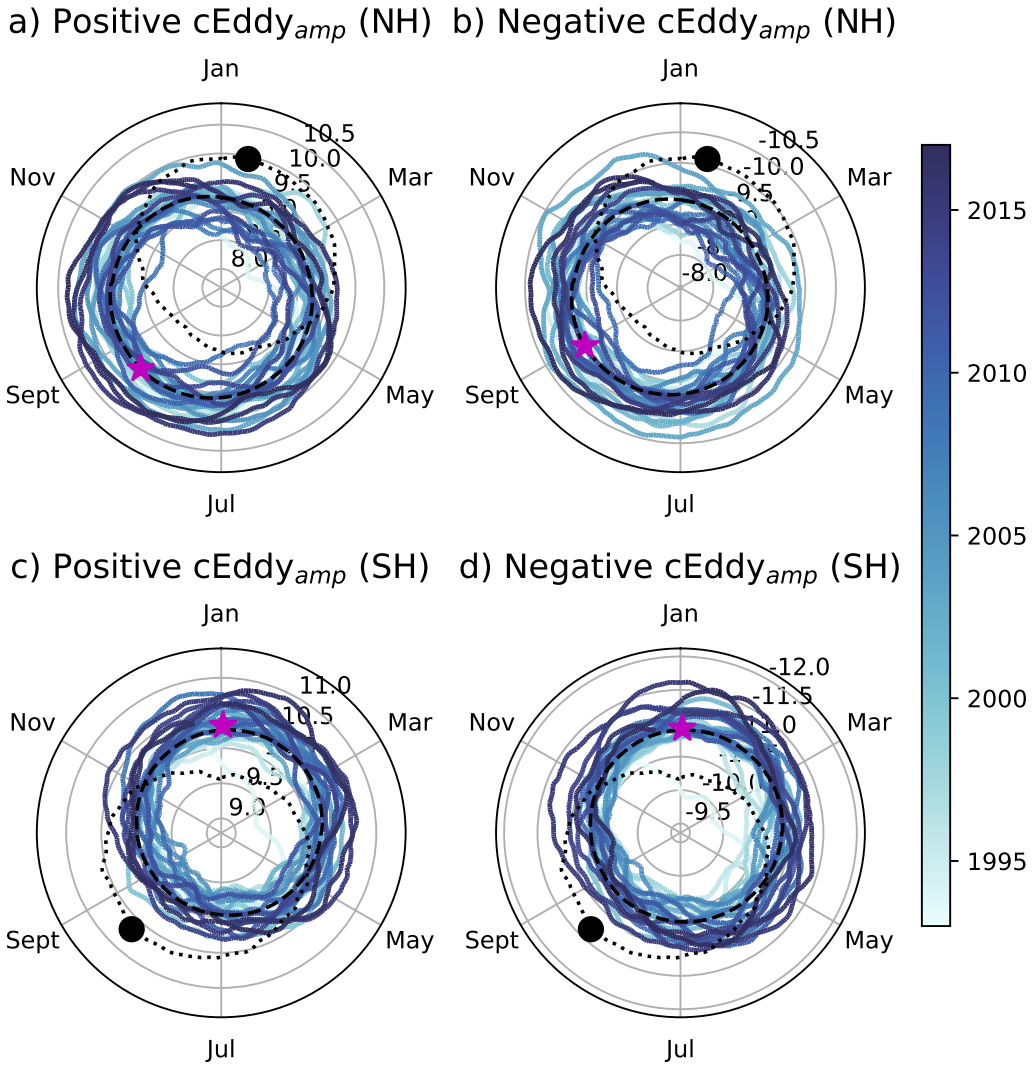
- 297 • The number and amplitude of coherent eddies from two eddy tracking algorithms
298 show consistent trend patterns.
- 299 • In particular, we observe a decrease in the number of eddies in the southern ocean,
300 as well as sectors in the North Atlantic and North Pacific.



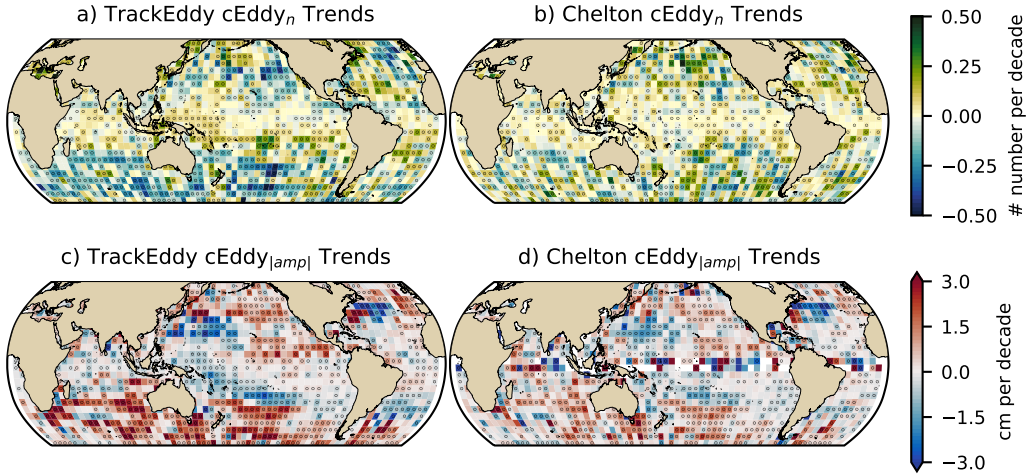
257 **Figure 5.** Climatology of the coherent eddy statistics. a) Climatology of the number of coher-
 258 ent eddies ($cEddy_n$) identified by Chelton et al. (2007); b) Climatology of the number of coher-
 259 ent eddies ($cEddy_n$) identified by Martínez-Moreno et al. (2019); c) Climatology of the mean abso-
 260 lute coherent eddy amplitude ($cEddy_{amp}$). d) Climatology of the mean coherent eddy amplitude
 261 ($cEddy_{amp}$).



275 **Figure 6.** Hemispherical seasonality of the coherent eddy statistics; a,e) seasonal cycle of the
 276 number of coherent eddies ($cEddy_n$); b,f) seasonal cycle of the mean coherent eddy amplitude
 277 ($cEddy_{amp}$); c,g) seasonal cycle of the warm core coherent eddies amplitude (positive $cEddy_{amp}$);
 278 d,h) seasonal cycle of the cold core coherent eddies amplitude (negative $cEddy_{amp}$). Panels a,b
 279 and c show the northern hemisphere seasonal cycle, while panels d,e, and f correspond to the
 280 southern hemisphere. Dashed lines correspond to the seasonal cycle of the fields and dotted lines
 281 show the seasonal cycle of the wind magnitude smoothed over 120 days (moving average). The
 282 green and magenta stars show the maximum of the seasonal cycle for each field and the wind
 283 magnitude, respectively. The line colors show the year.



286 **Figure 7.** Hemispherical seasonality of the coherent eddy statistics; a,e) seasonal cycle of the
 287 number of coherent eddies ($cEddy_n$); b,f) seasonal cycle of the mean coherent eddy amplitude
 288 ($cEddy_{amp}$); c,g) seasonal cycle of the warm core coherent eddies amplitude (positive $cEddy_{amp}$);
 289 d,h) seasonal cycle of the cold core coherent eddies amplitude (negative $cEddy_{amp}$). Panels a,b
 290 and c show the northern hemisphere seasonal cycle, while panels d,e, and f correspond to the
 291 southern hemisphere. Dashed lines correspond to the seasonal cycle of the fields and dotted lines
 292 show the seasonal cycle of the wind magnitude smoothed over 120 days (moving average). The
 293 green and magenta stars show the maximum of the seasonal cycle for each field and the wind
 294 magnitude, respectively. The line colors show the year.



306 **Figure 8.** Trends of coherent eddy statistics. a,b and c Trends of the number of identified
 307 coherent eddies from satellite observations identified using TrackEddy, satellite observations iden-
 308 tified using Chelton's, and state of the art numerical simulation identified using TrackEddy. d,e
 309 and f Trends of the sum of the absolute value of identified coherent eddies amplitude from satel-
 310 lite observations identified using TrackEddy, satellite observations identified using Chelton's, and
 311 state of the art numerical simulation identified using TrackEddy. Gray stippling shows regions
 312 that are statistically significant above the 95% confidence level.

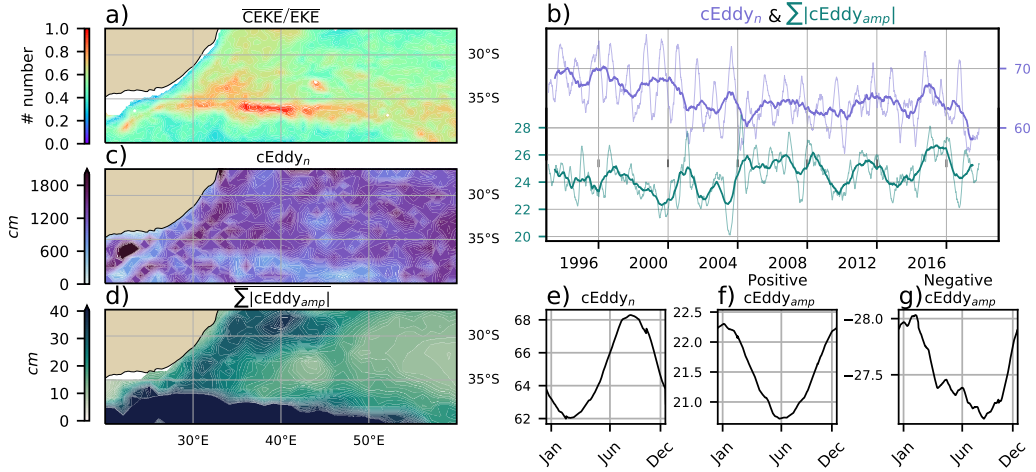
- 301 • Meanwhile the amplitude seems to be increasing in those same regions.
 302 • Some of these regions have undergone a readjustment to stronger winds, thus the
 303 observed trends in the eddy amplitude suggests an intensification of the coherent
 304 eddy field to an increase in the forcing.
 305 • This increase is consistent with Martínez-Moreno et al. (2021)

313 6 Regional

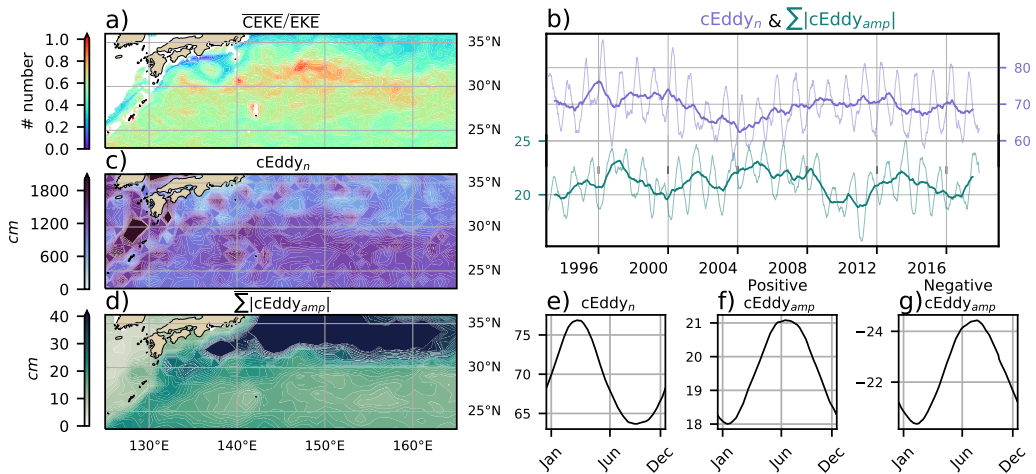
314 6.1 Boundary Currents

315 Figure 10

- 316 • Described similar to figure 7, 8, and 9
 317 • Note that boundary currents have a consistent seasonal cycle in the positive and
 318 negative eddy amplitude.
 319 • As expected, the seasonal cycle is opposite to BC in the northern hemisphere.



320

Figure 9. Same as Figure 12 but for the Agulhas Current.

325

Figure 10. Same as Figure 12 but for the Kuroshio Current.

321

Figure 11

322

- Described similar to figure 7, 8, and 9
- Note that boundary currents have a consistent seasonal cycle in the positive and negative eddy amplitude.

323

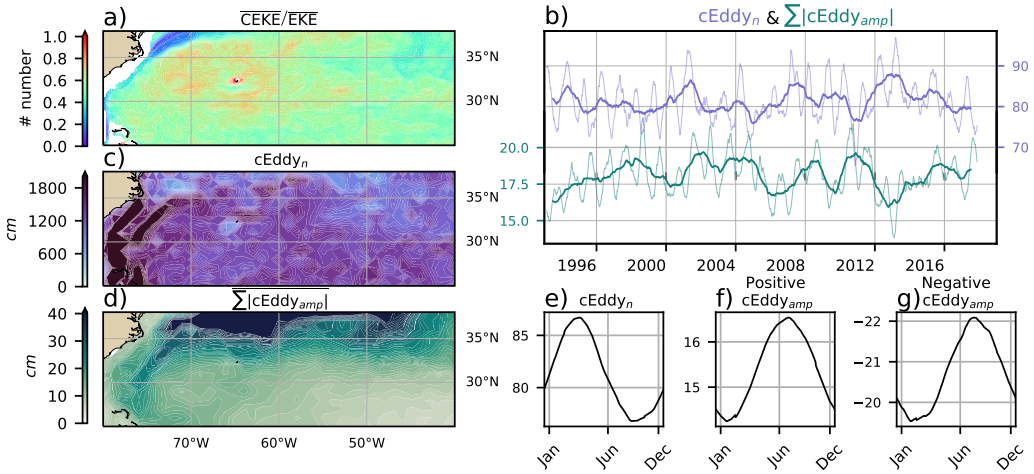
324

326

Figure 12

327

- Described similar to figure 7, 8, and 9



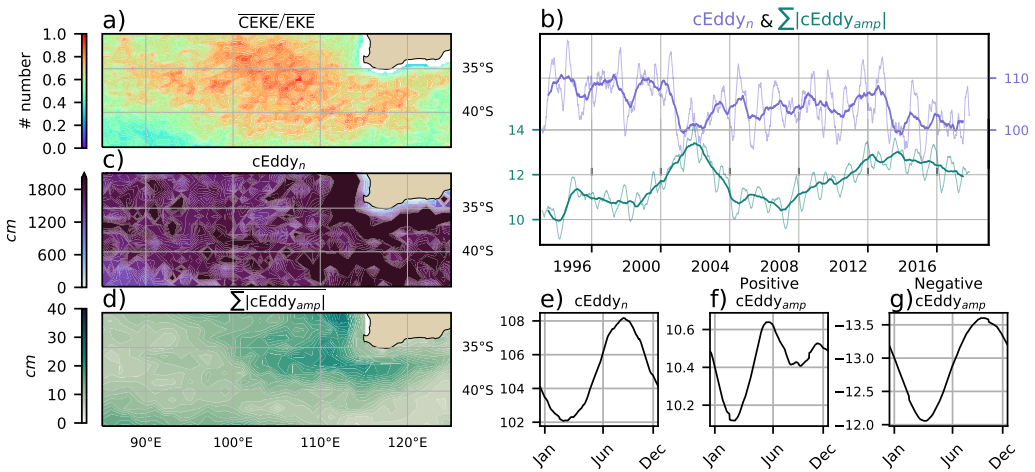
331 **Figure 11.** Move to supplementary Same as Figure 12 but for the Gulf Stream.

- 328 • Note that boundary currents have a consistent seasonal cycle in the positive and
329 negative eddy amplitude.
330 • Delete Fig 11 or 12, they are really similar. What do you think?

332 **6.2 Eastern currents**

333 **Figure 7**

- 334 • South of the Leeuwin Current there is an important dominance fo the coherent
335 eddy field, where it explains around 80% of the eddy kinetic energy.
336 • Although this region does not have a large EKE, we can observe a considerable
337 amount of eddies across the region, but more importantly the coherent eddy am-
338 plitude is particularly large in those regions with coherent eddy dominance.
339 • The solid lines show an decrease in the number of eddies, but an increase in the
340 eddy amplitude.
341 • Moreover, the coherent eddy number peaks in August.
342 • Meanwhile coherent eddies with the positive amplitude have a smaller amplitude
343 than the negative, furthermore, the positive eddies peak in Jun and show a inter-
344 annual modulation, while the negative eddies peak in October.
345 • Research regional dynamics (Add here why we may expect this response.)



346 **Figure 12.** Climatology of the eddy field and coherent eddy field at the Leeuwin Current. a)
 347 Ratio of mean coherent eddy kinetic energy ($\overline{\text{CEKE}}$) versus mean eddy kinetic energy ($\overline{\text{EKE}}$); b)
 348 Thick lines show the running average over 2 years and thin lines show the running average over
 349 90 days of the coherent eddy number sum and the average absolute coherent eddy amplitude; c)
 350 Map of the number of eddies; d) Map of the average absolute coherent eddy amplitude; e) Sea-
 351 sonal cycle of the number of eddies f) Seasonal cycle of the positive coherent eddy amplitude. g)
 352 Seasonal cycle of the negative coherent eddy amplitude.

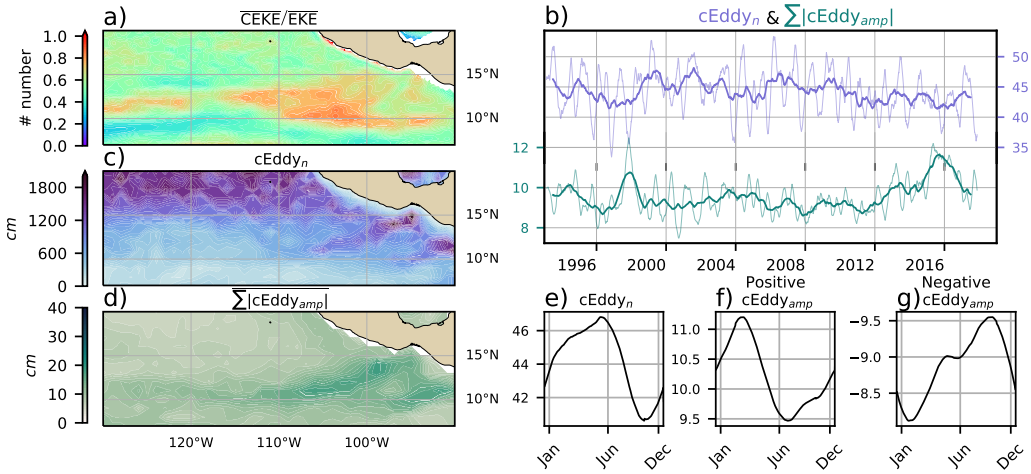


Figure 13. Same as Figure 12 but for the East Tropical Pacific.

361

Figure 9

354

- Here we observe that the number of eddies and eddy amplitude are large in the area where the coherent eddies dominate the eddy field.
- Dynamically, in this region eddies are generated due to Rossby wave propagation along the coast that becomes unstable and sheds eddies at the Tehuantepec Gulf.
- The seasonal cycle shows a peak in Jun, while the positive amplitude is observed in March and the negative amplitude maximum occurs in September.
- Research regional dynamics (Add here why we may expect this response.)

362

7 Summary and Conclusions

363

Acknowledgments

364

References

365

Arbic, B. K., Polzin, K. L., Scott, R. B., Richman, J. G., & Shriver, J. F. (2013).

366

On Eddy Viscosity, Energy Cascades, and the Horizontal Resolution of Gridded

367

Satellite Altimeter Products*. *Journal of Physical Oceanography*, 43(2), 283–300.

368

doi: 10.1175/jpo-d-11-0240.1

369

Ashkezari, M. D., Hill, C. N., Follett, C. N., Forget, G., & Follows, M. J. (2016).

- 370 Oceanic eddy detection and lifetime forecast using machine learning methods.
371 *Geophysical Research Letters*, 43(23). doi: 10.1002/2016gl071269
- 372 Beron-Vera, F. J., Wang, Y., Olascoaga, M. J., Goni, G. J., & Haller, G. (2013). Ob-
373 jective Detection of Oceanic Eddies and the Agulhas Leakage. *Journal of Physical*
374 *Oceanography*, 43(7), 1426–1438. doi: 10.1175/JPO-D-12-0171.1
- 375 Bouali, M., Sato, O. T., & Polito, P. S. (2017). Temporal trends in sea surface tem-
376 perature gradients in the South Atlantic Ocean. *Remote Sensing of Environment*,
377 194, 100–114. doi: 10.1016/j.rse.2017.03.008
- 378 Callies, J., Flierl, G., Ferrari, R., & Fox-Kemper, B. (2015). The role of mixed-layer
379 instabilities in submesoscale turbulence. *Journal of Fluid Mechanics*, 788, 5–41.
380 doi: 10.1017/jfm.2015.700
- 381 Cane, M. A., Clement, A. C., Kaplan, A., Kushnir, Y., Pozdnyakov, D., Seager, R.,
382 ... Murtugudde, R. (1997). Twentieth-Century Sea Surface Temperature Trends.
383 *Science*, 275(5302), 957–960. doi: 10.1126/science.275.5302.957
- 384 Chelton, D. B., Gaube, P., Schlax, M. G., Early, J. J., & Samelson, R. M. (2011).
385 The influence of nonlinear mesoscale eddies on near-surface oceanic chlorophyll.
386 *Science*, 334(6054), 328-32. doi: 10.1126/science.1208897
- 387 Chelton, D. B., Schlax, M. G., Samelson, R. M., & de Szoeke, R. A. (2007). Global
388 observations of large oceanic eddies. *Geophysical Research Letters*, 34(15),
389 L15606. doi: 10.1029/2007GL030812
- 390 CMEMS. (2017). The Ssalto/Duacs altimeter products were produced and dis-
391 tributed by the Copernicus Marine and Environment Monitoring Service. *Aviso*
392 *Dataset*. Retrieved from <https://www.aviso.altimetry.fr/>
- 393 Cui, W., Wang, W., Zhang, J., & Yang, J. (2020). Identification and census statis-
394 tics of multicore eddies based on sea surface height data in global oceans. *Acta*
395 *Oceanologica Sinica*, 39(1), 41–51. doi: 10.1007/s13131-019-1519-y
- 396 Faghmous, J. H., Frenger, I., Yao, Y., Warmka, R., Lindell, A., & Kumar, V. (2015,
397 6). A daily global mesoscale ocean eddy dataset from satellite altimetry. *Scientific*
398 *Data*, 2, 150028 EP -. doi: 10.1038/sdata.2015.28
- 399 Ferrari, R., & Wunsch, C. (2009). Ocean Circulation Kinetic Energy: Reservoirs,
400 Sources, and Sinks. *Annual Review of Fluid Mechanics*, 41(1), 253–282. doi: 10
401 .1146/annurev.fluid.40.111406.102139
- 402 Frenger, I., Gruber, N., Knutti, R., & Münnich, M. (2013). Imprint of Southern

- 403 Ocean eddies on winds, clouds and rainfall. *Nature Geoscience*, 6(8), 608 EP -.
404 doi: 10.1038/ngeo1863
- 405 Frenger, I., Münnich, M., Gruber, N., & Knutti, R. (2015). Southern Ocean eddy
406 phenomenology. *Journal of Geophysical Research: Oceans*, 120(11), 7413-7449.
407 doi: 10.1002/2015JC011047
- 408 Fu, L., Chelton, D., Le Traon, P., & Oceanography, M. R. (2010). Eddy dynamics
409 from satellite altimetry. *Oceanography*, 23(4), 14-25. doi: 10.2307/24860859
- 410 Gill, A., Green, J., & Simmons, A. (1974). Energy partition in the large-scale ocean
411 circulation and the production of mid-ocean eddies. *Deep Sea Res Oceanogr Abstr*,
412 21(7), 499-528. doi: 10.1016/0011-7471(74)90010-2
- 413 Hogg, A. M., & Blundell, J. R. (2006). Interdecadal variability of the southern
414 ocean. *Journal of Physical Oceanography*, 36(8), 1626-1645. doi: 10.1175/
415 JPO2934.1
- 416 Hogg, A. M., Meredith, M. P., Chambers, D. P., Abrahamsen, E. P., Hughes,
417 C. W., & Morrison, A. K. (2015). Recent trends in the Southern Ocean
418 eddy field. *Journal of Geophysical Research: Oceans*, 120(1), 257-267. doi:
419 10.1002/2014JC010470
- 420 Hu, S., Sprintall, J., Guan, C., McPhaden, M. J., Wang, F., Hu, D., & Cai,
421 W. (2020, 2). Deep-reaching acceleration of global mean ocean circula-
422 tion over the past two decades. *Science Advances*, 6(6), eaax7727. doi:
423 10.1126/sciadv.aax7727
- 424 Kang, D., & Curchitser, E. N. (2017). On the Evaluation of Seasonal Variability of
425 the Ocean Kinetic Energy. *Geophysical Research Letters*, 47, 1675-1583. doi: 10
426 .1175/JPO-D-17-0063.1
- 427 Li, G., Cheng, L., Zhu, J., Trenberth, K. E., Mann, M. E., & Abraham, J. P. (2020).
428 Increasing ocean stratification over the past half-century. *Nature Climate Change*,
429 1–8. doi: 10.1038/s41558-020-00918-2
- 430 Martínez-Moreno, J., Hogg, A. M., England, M., Constantinou, N. C., Kiss, A. E.,
431 & Morrison, A. K. (2021). Global changes in oceanic mesoscale currents over the
432 satellite altimetry record. *Journal of Advances in Modeling Earth Systems*, 0(ja).
433 doi: 10.1029/2019MS001769
- 434 Martínez-Moreno, J., Hogg, A. M., Kiss, A. E., Constantinou, N. C., & Mor-
435 rison, A. K. (2019). Kinetic energy of eddy-like features from sea surface

- 436 altimetry. *Journal of Advances in Modeling Earth Systems*, 0(ja). doi:
437 10.1029/2019MS001769

438 Patel, R. S., Llort, J., Strutton, P. G., Phillips, H. E., Moreau, S., Pardo, P. C.,
439 & Lenton, A. (2020). The Biogeochemical Structure of Southern Ocean
440 Mesoscale Eddies. *Journal of Geophysical Research: Oceans*, 125(8). doi:
441 10.1029/2020jc016115

442 Pilo, G. S., Mata, M. M., & Azevedo, J. L. L. (2015). Eddy surface properties and
443 propagation at Southern Hemisphere western boundary current systems. *Ocean
444 Science*, 11(4), 629–641. doi: 10.5194/os-11-629-2015

445 Qiu, B. (1999). Seasonal Eddy Field Modulation of the North Pacific Subtropical
446 Countercurrent: TOPEX/Poseidon Observations and Theory. *Journal of Physical
447 Oceanography*, 29(10), 2471–2486. doi: 10.1175/1520-0485(1999)029<2471:sefmot>2
448 .0.co;2

449 Qiu, B., & Chen, S. (2004). Seasonal Modulations in the Eddy Field of the South
450 Pacific Ocean. *Journal of Physical Oceanography*, 34(7), 1515–1527. doi: 10.1175/
451 1520-0485(2004)034<1515:smitef>2.0.co;2

452 Qiu, B., Chen, S., Klein, P., Sasaki, H., & Sasai, Y. (2014). Seasonal Mesoscale
453 and Submesoscale Eddy Variability along the North Pacific Subtropical Coun-
454 tercurrent. *Journal of Physical Oceanography*, 44(12), 3079–3098. doi:
455 10.1175/jpo-d-14-0071.1

456 Ruela, R., Sousa, M. C., deCastro, M., & Dias, J. M. (2020). Global and regional
457 evolution of sea surface temperature under climate change. *Global and Planetary
458 Change*, 190, 103190. doi: 10.1016/j.gloplacha.2020.103190

459 Sasaki, H., Klein, P., Qiu, B., & Sasai, Y. (2014). Impact of oceanic-scale inter-
460 actions on the seasonal modulation of ocean dynamics by the atmosphere. *Nature
461 Communications*, 5(1), 5636. doi: 10.1038/ncomms6636

462 Schubert, R., Schwarzkopf, F. U., Baschek, B., & Biastoch, A. (2019). Submesoscale
463 Impacts on Mesoscale Agulhas Dynamics. *Journal of Advances in Modeling Earth
464 Systems*, 11(8), 2745–2767. doi: 10.1029/2019ms001724

465 Siegel, D., Peterson, P., DJ, M., Maritorena, S., & Nelson, N. (2011). Bio-optical
466 footprints created by mesoscale eddies in the Sargasso Sea. *Geophysical Research
467 Letters*, 38(13), n/a-n/a. doi: 10.1029/2011GL047660

468 Uchida, T., Abernathey, R., & Smith, S. (2017). Seasonality of eddy kinetic energy

- 469 in an eddy permitting global climate model. *Ocean Modelling*, 118, 41-58. doi: 10
470 .1016/j.ocemod.2017.08.006
- 471 Wunsch, C. (2020). Is The Ocean Speeding Up? Ocean Surface Energy Trends.
472 *Journal of Physical Oceanography*, 50(11), 1–45. doi: 10.1175/jpo-d-20-0082.1
- 473 Wunsch, C., & Ferrari, R. (2004). VERTICAL MIXING, ENERGY, AND THE
474 GENERAL CIRCULATION OF THE OCEANS. *Annual Review of Fluid Me-
475 chanics*, 36(1), 281–314. doi: 10.1146/annurev.fluid.36.050802.122121
- 476 Wyrtki, K., Magaard, L., & Hager, J. (1976). Eddy energy in the oceans. *Journal of
477 Geophysical Research*, 81(15), 2641-2646. doi: 10.1029/JC081i015p02641